Solution Conformation of the (−)-*cis*-*anti*-Benzo[*a*]pyrenyl-dG Adduct Opposite dC in a DNA Duplex: Intercalation of the Covalently Attached BP Ring into the Helix with Base Displacement of the Modified Deoxyguanosine into the Major Groove[†]

Monique Cosman,[‡,§] Brian E. Hingerty,[||] Natalia Luneva,[⊥] Shantu Amin,[#] Nicholas E. Geacintov,[⊥] Suse Broyde,[▽] and Dinshaw J. Patel*,[‡]

Cellular Biochemistry and Biophysics Program, Memorial Sloan Kettering Cancer Center, New York, New York 10021, Health Sciences Research Division, Oak Ridge National Laboratory, Oak Ridge, Tennessee 37831, Chemistry and Biology Departments, New York University, New York, New York 10003, and American Health Foundation, Valhalla, New York 10595

Received March 4, 1996; Revised Manuscript Received May 8, 1996[⊗]

ABSTRACT: This paper reports on the combined NMR−molecular mechanics computational studies of the solution structure of the (−)-*cis*-*anti*-[BP]dG adduct positioned opposite dC in the sequence context d(C1-C2-A3-T4-C5-[BP]G6-C7-T8-A9-C10-C11)·d(G12-G13-T14-A15-G16-C17-G18-A19-T20-G21-G22) duplex [designated (−)-*cis*-*anti*-[BP]dG·dC 11-mer duplex]. This adduct is derived from *cis* addition at C^{10} of (−)-*anti*-7(*S*),8(*R*)-dihydroxy-9(*R*),10(*S*)-epoxy-7,8,9,10-tetrahydrobenzo[*a*]pyrene [(−)-*anti*-BPDE] to the N^2 position of dG6 in this duplex sequence. The exchangeable and nonexchangeable protons of the benzo[*a*]pyrenyl moiety and nucleic acid of the major conformation were assigned following analysis of two-dimensional NMR data sets in H_2O and D_2O solution. There was a general broadening of proton resonances for a three-nucleotide segment centered about the lesion site which resulted in a tentative assignment for the sugar protons of the C7 residue in the spectrum of the adduct duplex. The solution conformation of the major conformation of the (−)-*cis*-*anti*-[BP]dG·dC 11-mer duplex has been determined by incorporating DNA−DNA and intermolecular BP-DNA proton−proton distances defined by lower and upper bounds deduced from NOESY data sets as restraints in molecular mechanics computations in torsion angle space. The results establish that the covalently attached benzo[*a*]pyrenyl ring intercalates between intact Watson−Crick dC5·dG18 and dC7·dG16 base pairs. The modified deoxyguanosine [BP]-dG6 and its partner cytosine dC17 are looped out of the helix into the major groove. The purine ring of the [BP]dG6 residue is directed toward the 5′-end of the modified strand and stacks over the major groove edge of its 5′-side neighbor dC5 residue. The solution structure of the (−)-*cis*-*anti*-[BP]dG·dC 11-mer duplex is compared with those of the stereoisomeric (+)-*trans*-*anti*-[BP]dG [Cosman, M., et al. (1992) *Proc. Natl. Acad. Sci. U.S.A. 89*, 1914−1918], (−)-*trans*-*anti*-[BP]dG [de los Santos, C., et al. (1992) *Biochemistry 31*, 5245−5252], and (+)-*cis*-*anti*-[BP]dG [Cosman, M., et al. (1993a) *Biochemistry 32*, 4146−4155] adducts positioned opposite dC in the same duplex sequence context. A key finding is that the long axes of the intercalated benzo[*a*]pyrenyl rings in the solution structures of the (+)- and (−)-*cis*-*anti*-[BP]dG·dC 11-mer duplexes are oriented in opposite directions with the benzylic ring directed toward the minor groove in the (+)-*cis* isomer and toward the major groove in the (−)-*cis* isomer. In addition, a comparison is also made with the solution structure of the (+)-*trans*-*anti*-[BP]dG adduct opposite a deletion site [Cosman, M., et al. (1994a) *Biochemistry 33*, 11507−11517] since this adduct duplex displays several conformational features in common with the structure of the (−)-*cis*-*anti*-[BP]dG·dC 11-mer duplex. The structures of both duplex adducts exhibit intercalation of the covalently attached ligand into the helix and displacement of the modified deoxyguanosine into the major groove. Studies of the biological activities of stereochemically defined BP-DNA adducts and the comparison of the solution structure of the (−)-*cis*-*anti*-[BP]dG·dC 11-mer duplex with its stereoisomeric counterparts should lead to new insights into the relationships between defined helical distortions and mutagenic specificity and activity.

The stereochemical properties of biologically active compounds can profoundly influence their interactions with cellular molecules. Well known examples include the metabolic stereoselective synthesis of oxygenated polycyclic aromatic derivatives (Conney, 1982; Singer & Grunberger, 1983), chiral recognition in xenobiotic metabolism and drug−receptor interactions (Testa, 1989), ligand−DNA interactions (Barton, 1989), the pharmacology of drug

[†] This research is supported by NIH Grant CA-46533 to D.J.P., by NIH Grant CA-20851 and DOE Grant DE-FG02-88ER60405 to N.E.G., by NIH Grant CA-28038, NIH Grant RR-06458, and DOE Grant DE-FG02-90ER60931 to S.B., and by DOE Contract DE-AC05-960R22464 with Lockheed Martin Energy Research and DOE-OHER Field Work Proposal ERKP931 to B.E.H.

[‡] Memorial Sloan Kettering Cancer Center.
[§] Present address: Biology & Biotechnology Research Program, Lawrence Livermore National Laboratory, Livermore, CA 94550.
[||] Oak Ridge National Laboratory.
[⊥] Chemistry Department, New York University.
[#] Biology Department, New York University.
[▽] American Health Foundation.

[⊗] Abstract published in *Advance ACS Abstracts,* July 1, 1996.

S0006-2960(96)00534-X CCC: $12.00

molecules (Campbell & Wilson, 1991; Stinson, 1995), and the genotoxic, mutagenic, and tumorigenic properties of a variety of metabolites of polycyclic aromatic compounds (Conney, 1982; Seiler, 1990).

A specific and well studied example of the interrelationship between stereochemistry and biological activity is the difference in the tumorigenic and mutagenic potencies of the (+)-7*R*,8*S*,9*S*,10*R* and (−)-7*S*,8*R*,9*R*,10*S* enantiomers of *anti*-7,8-dihydroxy-9,10-epoxy-7,8,9,10-tetrahydrobenzo[*a*]pyrene [(+)- and (−)-*anti*-BPDE, respectively]. Benzo[*a*]pyrene is an environmental carcinogen that is present in products generated from fossil fuel combustion, tobacco smoke, and certain methods of cooking (Phillips, 1987). It can be metabolically activated by cellular P-450 enzymes to (+)- and (−)-*anti*-BPDE (Sims et al., 1974), each of which display striking differences in their biological activities (Levin et al., 1976; Wood et al., 1977; Kapitulnik et al., 1978; Stevens et al., 1985). While (+)-*anti*-BPDE is highly tumorigenic on mouse skin and in newborn mouse lung, the (−)-enantiomer is not (Buening et al., 1978; Slaga et al., 1979). In addition, the (+)-isomer is more mutagenic in mammalian cells, while (−)-*anti*-BPDE is more active in bacterial cells (Wood et al., 1977; Brookes & Osborne, 1982; Stevens et al., 1985).

The formation of covalent DNA adducts is widely believed to account for the observed mutagenic and tumorigenic activities of the benzo[*a*]pyrene diol epoxides (Meehan & Straub, 1979; Singer & Grunberger, 1983; Arce & Grunberger, 1983; Ashurst et al., 1983; Arce et al., 1987; Harvey & Geacintov, 1987; Cheng et al., 1989). This in turn has engendered considerable interest in determining the relationship between the conformations of the stereochemically distinct BP-DNA adducts and their specific mutagenic activities. Each (+)- and (−)-*anti* enantiomer can bind covalently to the exocyclic amino group of guanine or adenine by either *trans* or *cis* addition at the C^{10} carbon yielding a total of eight adducts. Although the *trans*-N^2-dG adducts are the major products (Jeffrey et al., 1976; Cheng et al., 1989), the tumorigenic and mutagenic potentials of the minor products may also be of critical importance in the expression of the biological activity of the parent *anti*-BPDEs.

Thus, a systematic study of the relationship between the structures of these BP-DNA adducts and their biological activities should result in a greater understanding of the mechanism of carcinogenesis initiated by these compounds. There have been several recent studies reported in the literature of the solution structures of stereochemically defined deoxyoligonucleotide adducts derived from the binding of benzo[*a*]pyrene diol epoxides to either dG or dA. These include the (+)-*trans-anti*-[BP]dG adduct positioned opposite a dC residue (Cosman et al., 1992; Fountain & Krugh, 1995) and a deletion site (Cosman et al., 1994a) or at a template−primer junction (Cosman et al., 1995c), the (−)-*trans-anti*-[BP]dG·dC 11-mer duplex (de los Santos et al., 1992), the (+)-*cis-anti*-[BP]dG adduct positioned opposite a dC residue (Cosman et al., 1993a), and a deletion site (Cosman et al., 1994b) as well as (−)-*trans-anti*-[BP]-dA·dG (Schurter et al., 1995a), (+)-*trans-anti*-[BP]dA·dG (Yeh et al., 1995), and the (−)-*trans-syn*-[BP]dA·dT (Schurter et al., 1995b) duplex adducts.

The present combined NMR energy-minimization study of the (−)-*cis-anti*-[BP]dG·dC 11-mer duplex completes the determination of the solution structures of the four possible DNA adducts obtained from the *cis* and *trans* addition at the N^2 position of dG by the enantiomeric (+)- and (−)-*anti*-BPDEs. The (−)-*cis-anti*-[BP]dG6 residue (**1**) is positioned opposite dC17 and flanked by dC5·dG18 and dC7·dG16 pairs in the same DNA sequence context (**2**) used in our previous studies of the (+)-*trans*-, (−)-*trans*-, and (+)-*cis-anti*-[BP]dG·dC 11-mer duplexes.

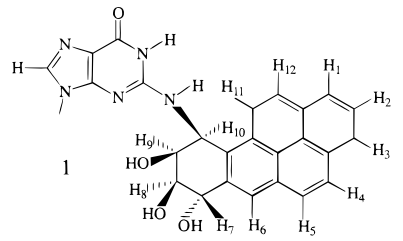

1

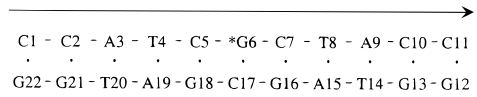

2

MATERIALS AND METHODS

Preparation of the (−)-cis-anti-[BP]-dG·dC 11-mer. Racemic *anti*-BPDE was synthesized by previously published methods. The synthesis of the (−)-*cis-anti*-BP-N^2-dG covalent adduct in the d(C-C-A-T-C-[BP]G-C-T-A-C-C) sequence was carried out using previously described methods (Cosman et al., 1990) starting, however, with (±)-*anti*-BPDE. The (+)-*trans*-, (−)-*trans*, (+)-*cis*, and (−)-*cis-anti*-[BP]dG isomeric covalent adducts at the 11-mer strand level were separable by preparative HPLC on a C18 ODS Hypersil column (Cosman et al., 1990). The enantiomerically pure modified (−)-*cis-anti*-[BP]dG 11-mer d(C-C-A-T-C-[BP]G-C-T-A-C-C) strand was annealed to the complementary unmodified 11-mer d(G-G-T-A-G-C-G-A-T-G-G) strand at 70 °C, and the stoichiometry was followed by monitoring single proton resonances in both strands. The melting point of this duplex is 46.0 ± 0.5 °C at 10 μM strand concentration (Ya et al., 1994).

NMR Experiments. A combination of through-space nuclear Overhauser effect (NOESY) and through-bond correlated (COSY, TOCSY) two-dimensional spectra were recorded on approximately 4 mg of the (−)-*cis-anti*-[BP]-dG·dC 11-mer in either 0.6 or 0.35 mL (using a Shigemi microtube, Allison Park, PA) of 0.1 M NaCl, 10 mM phosphate, pH 7.0, aqueous buffer and analyzed in order to assign the BP and nucleic acid protons. All experiments were carried out using a Varian Unity Plus 600 MHz instrument in the States−TPPI mode (Marion et al., 1989) with a 2.0 s relaxation delay between scans. The temperature of the sample was calibrated with an external methanol sample. The NOESY spectrum (150 ms mixing time) of the adduct duplex in H_2O buffer at 1 °C was collected using a jump−return pulse for solvent suppression and NOESY spectra as a function of mixing time were collected in D_2O buffer at 10 °C. The through-bond TOCSY data sets in D_2O

buffer were recorded at spin lock times of 40 and 80 ms at 10 °C.

Several factors went into the conversion of the NOE intensities into the distance bounds used for the structure determination of the adduct duplex. Distance restraints involving nonexchangeable protons were estimated from NOE buildup curves of NOESY spectra recorded at 40, 80, 120, 160, 200, and 240 ms on the adduct duplex in D_2O. The interproton distance calculations were based on the isolated two-spin approximation using the dT(NH3)−dA-(H2) fixed distance of 2.92 Å for the NOESY spectra in H_2O and the dC(H6)−dC(H5) fixed distance of 2.45 Å for the NOESY data sets in D_2O solution. The choice of upper and lower bound ranges on the estimated distances depended on the resolution of the cross peaks in the contour plots. The base proton to sugar H1′ proton NOE cross peaks in the shortest mixing time NOESY data set in D_2O were evaluated to qualitatively differentiate between *syn* (strong NOE) and *anti* (weak NOE) glycosidic torsion angles (Patel et al., 1982).

The proton−proton vicinal coupling constants among sugar protons were analyzed from phase-sensitive COSY spectra to qualitatively distinguish between the C3′-*endo* and C2′-*endo* family of sugar puckers. The relative intensity of the NOE cross peaks between base protons and their own and 5′-flanking sugar H2′, H2″, and H3′ protons were used to qualitatively distinguish between the A and B family of helices for the modified duplex (van der Ven & Hilbers, 1988).

Molecular Mechanics Computations. We employ our own molecular mechanics program DUPLEX (Hingerty et al., 1989), which has been especially tailored for investigating the conformations of carcinogen−DNA adducts. One key feature of DUPLEX is that it employs a consistent force field for both the carcinogen and the DNA. The DNA force field is essentially one developed in the laboratory of Olson (Taylor & Olson, 1983), and all carcinogen parameters, including the partial charge set, are consistent with it. This allows the force field to play a part in an interactive way, as described below, in the modeling of the structure. Force field parameters, including partial charges, for the (−)-*cis*-*anti*-[BP]dG are the same as those used for the (+)-*cis*-*anti*-[BP]dG stereoisomer (Cosman et al., 1993a). The conformation of the benzylic ring was in the distorted half-chair form with the BP(H7), BP(H8), and BP(H10) protons in the pseudoequatorial domain and the BP(H9) proton in the pseudoaxial domain, analogous to the conformation found in the (+)-*cis*-*anti*-[BP]dG stereoisomer (Cosman et al., 1993a).

In addition to the consistent force field, we employ special strategies to address the multiple minimum problem, which hinders locating the lowest energy structure on the potential energy surface. We employ energy minimization searches using the reduced variable domain of torsion angle space, also known as internal coordinates. The advantage of torsion space, compared to Cartesian space minimizations, is the vast diminution in the number of variables that must be simultaneously optimized, thereby permitting larger movements from a given starting conformation during minimization as well as assurance of realistic internal geometry (Hingerty et al., 1989). The energy minimization searches of the carcinogen−DNA orientation space employ starting structures with arbitrary, unbiased high energy carcinogen−DNA orientations. Typically, the two carcinogen−DNA torsion angles are surveyed at 90° intervals of each, in combination, for a total of 16 trials in one set.

Penalty functions or pseudo-potential energies (restraints) are employed as additions to the energy function, but only to guide the minimizer in the direction of the observed structure on the multidimensional hill and valley terrain of the potential energy surface. For restraints derived from NMR data, upper and lower bounds are included, using the following functions:

$$F_N = W_N \sum_1^n (d - d_N)^2 \quad (1)$$

$$F_{NN} = W_{NN} \sum_1^n (d - d_{NN})^2 \quad (2)$$

The *W*'s are adjustable weights (in the range of 10−30 kcal/mol·Å^2), d is the current value of the interproton distance, d_N is a target upper bound, and d_{NN} is a target lower bound. The summation is over all n NMR-derived distance bounds. Equation 1 is implemented when d is greater than d_N, and eq 2 is implemented when d is less than d_{NN}. F_N and F_{NN} can also be employed as goodness-of-fit indices to compare the quality of computed structures with respect to the NMR data. Here the d values are the achieved distances in a given model and the *W*'s are the weights employed in the search. F_N and F_{NN} are composites, reflecting the overall fit of all the achieved distances to their targets. They both adopt values of zero when all model distances are within the upper and lower NMR distance bounds. An important aspect of our use of these functions is the assigned value for *W*. Its value is chosen so that both the penalty function and the potential energy play their part. Thus, with an appropriate weight, the pseudopotentials contribute sufficiently to the energy function to guide the minimizer to target geometries without overwhelming the intrinsic potential energy.

DUPLEX features an additional unique hydrogen bond penalty function (Hingerty et al., 1989) that is extremely useful for locating structures with unusual hydrogen bonding patterns or disrupted hydrogen bonding sites. The function can be employed to search for structures with any selected hydrogen bonding pattern or disruption between any designated residues on either strand.

Our search strategy employs a limited set of key NMR distance restraints (in the range of one dozen to several dozen), together with information from the NMR data on the hydrogen bonding pattern between bases for the hydrogen bond penalty function. NMR information about the glycosidic torsion angle and the deoxyribose sugar pseudorotation parameter can also be included. The resulting structures are ranked according to energy and goodness of fit (eqs 1 and 2). At this point the first set of NMR assigned distance bounds are evaluated in relation to achieved distances and energies in the ensemble of 16 structures. Importantly, cross-checks involving distances not employed as restraints, including DNA−DNA distances, and satisfaction of other criteria such as chemical shifts are also made. Especially in the case of conformational heterogeneity, this affords feedback to the NMR analysis and offers the opportunity for reassessment of the distance bounds. This procedure can

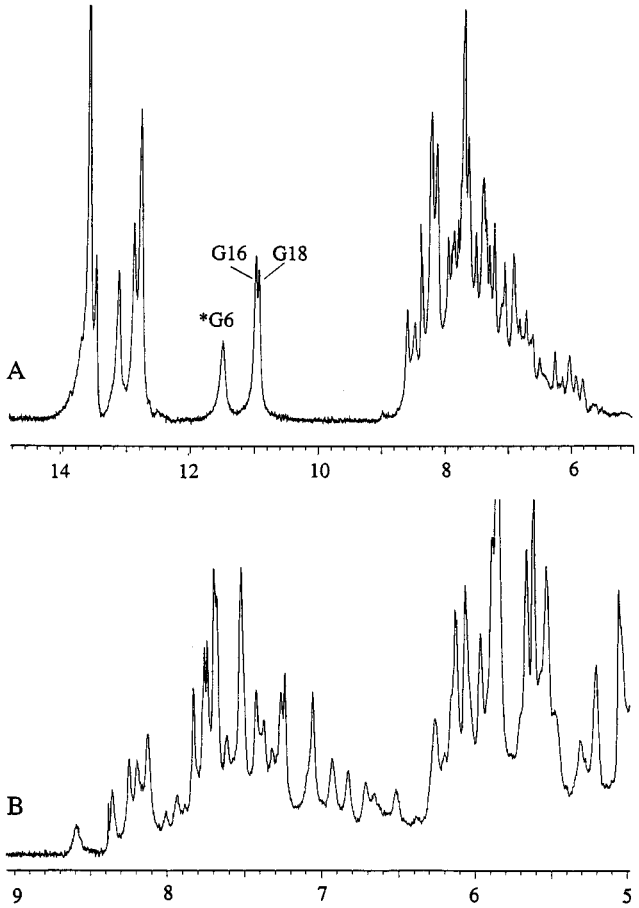

FIGURE 1: Proton NMR spectra of the (−)-*cis-anti*-[BP]dG·dC 11-mer duplex in 0.1 M NaCl, 10 mM phosphate, and 0.1 mM EDTA, aqueous solution, pH 7.0. (A) Exchangeable imino proton spectrum (5.6−14.8 ppm) in H_2O buffer at 1 °C. Selective imino proton assignments are recorded over the spectrum. (B) Nonexchangeable proton spectrum (5.0−9.0 ppm) in D_2O buffer at 10 °C.

be carried out interactively until structures of lowest energy and best goodness of fit are located. The structures with the best fit to the data are also usually among the lowest in energy. A family of such structures is usually found. Finally, the best subunit is built to the larger modified duplex with all restraints, and then all penalty functions are released to yield final unrestrained minimum energy structures in accord with the data. If final structures do not retain features consistent with the NMR data, further searches are performed.

Computations were carried out at the Department of Energy's National Energy Research Supercomputer Center and the National Science Foundation's San Diego Supercomputer Center.

RESULTS

Exchangeable Nucleic Acid Protons. The exchangeable proton NMR spectrum (5.6−14.8 ppm) of the (−)-*cis-anti*-[BP]dG·dC 11-mer in H_2O buffer, pH 7.0, at 1 °C is plotted in Figure 1A. Three upfield-shifted resonances at 10.94, 10.98, and 11.50 ppm are observed in addition to the partially resolved imino resonances between 12.7 and 13.6 ppm. These imino protons have been assigned following analysis of NOE connectivities between them and nearby protons both across the base pair and to the flanking base pairs [reviewed in Patel et al. (1987) and van der Ven and Hilbers (1988)].

An expanded NOESY (150 ms mixing time) contour plot of the symmetrical 10.3−14.1 ppm region (Figure 2A) establishes connectivities between adjacent base pairs in the (−)-*cis-anti*-[BP]dG·dC 11-mer duplex from the dC1·dG22 pair located at one end of the helix to the dC5·dG18 pair located 5′ to the [BP]dG6·dC17 modified pair and from the 3′-neighbor dC7·dG16 pair to the dC11·dG12 pair located at the opposite end of the helix. The NOE connectivities between the imino protons of dG16, [BP]dG6, and dG18 are not observed, although these residues are located at adjacent base pairs along the duplex sequence.

An expanded plot of the 150 ms mixing time NOESY spectrum of the (−)-*cis-anti*-[BP]dG·dC 11-mer duplex correlating connectivities between the imino protons (10.3 −14.1 ppm) and the base and amino protons (4.3−8.7 ppm) is plotted in Figure 2B. The observed NOE patterns establish Watson−Crick base pairing at all dA·dT pairs (deoxythymidine imino to deoxyadenosine H2 across the dA·dT pairs (peaks A−C, Figure 2B) and at all dG·dC pairs (deoxyguanosine imino to deoxycytidine amino across the dG·dC pairs), as shown for the dC5·dG18 and dC7·dG16 pairs (peaks F,F′ and E,E′, respectively, Figure 2B), with the exception of the alignment of the [BP]dG6·dC17 pair at the modification site (Figure 2B).

The narrow upfield-shifted imino proton of dG18 (10.94 ppm) flanking the lesion site exhibits NOE cross peaks to the upfield-shifted (6.64 and 5.52 ppm) amino protons of dC5 (peaks F and F′, Figure 2). Similarly, the narrow upfield-shifted imino proton of dG16 (10.98 ppm) which also flanks the lesion site exhibits NOE cross peaks to the exposed and upfield-shifted hydrogen-bonded (6.62 and 6.77 ppm) amino protons of dC7 (peaks E′ and E, respectively, Figure 2). These results establish formation of stable dC5·dG18 and dC7·dG16 base pairs on either side of the [BP]dG6 lesion positioned opposite dC.

The broad upfield-shifted imino proton at 11.50 ppm is assigned to [BP]dG6 in the adduct duplex. This imino proton is not hydrogen bonded to its partner dC17 and exchanges rapidly with solvent (peak D, Figure 2B), and we do not detect NOEs between it and other protons in the NOESY contour plot (Figure 2). The corresponding amino proton of [BP]dG6 is tentatively assigned to an exchangeable resonance at 8.62 ppm (peak A, Supporting Information, Figure S1), which overlaps with the nonexchangeable resonance of BP(H11). Both the upfield chemical shift and the larger line width of the imino resonance of [BP]dG6 suggest that this proton is not hydrogen-bonded and is accessible to solvent.

The exchangeable imino and amino proton chemical shifts are listed for the central d(T4-C5-[BP]G6-C7-T8)·d(A15-G16-C17-G18-A19) segment of the (−)-*cis-anti*-[BP]dG·dC 11-mer duplex at 1 °C in Table 1, and for the entire adduct duplex in the Supporting Information Table S1.

Nonexchangeable Nucleic Acid Protons. The base and sugar H1′ nonexchangeable proton spectrum region (5.0−9.0 ppm) of the (−)-*cis-anti*-[BP]dG·dC 11-mer duplex in D_2O buffer, pH 7.0 at 10 °C exhibits a mixture of narrow and broad resonances (Figure 1B). Data were obtained at low temperature due to loss of resolution on raising the temperature to ambient values. Nonexchangeable proton assignments were based on an analysis of through-space NOESY data sets (50 and 300 ms mixing times) and through-bond TOCSY data sets (40 and 80 ms spin lock times) at 10

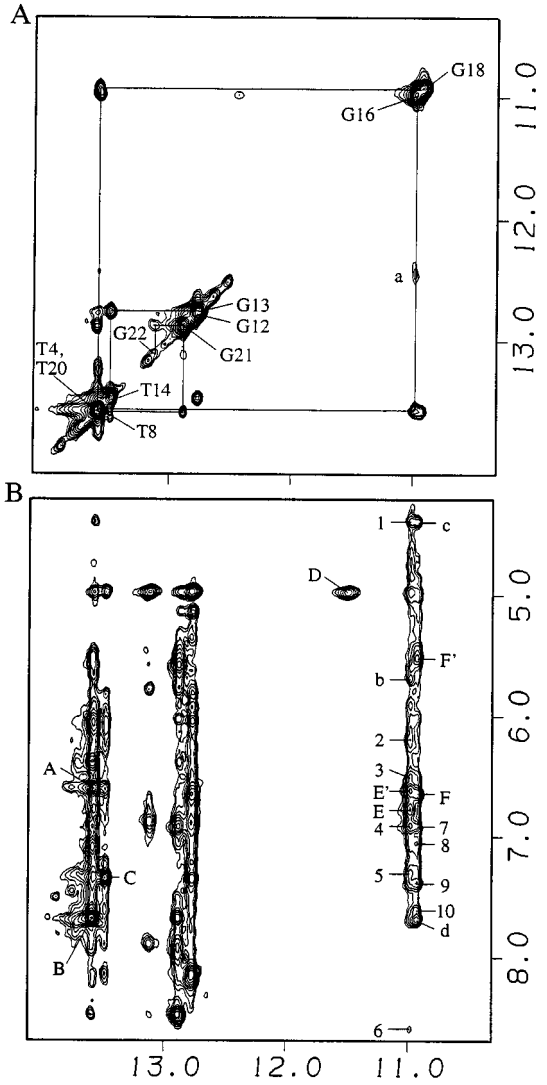

FIGURE 2: Expanded NOESY (150 ms mixing time) contour plots of the (−)-*cis-anti*-[BP]dG·dC 11-mer duplex in H_2O buffer at 1 °C. (A) NOE connectivities between adjacent base pairs in the symmetrical 10.3−14.1 ppm region are traced starting at dG22 located at one end of the helix and proceeding to dG18 located 5′ to [BP]dG6 and from dG16 located 3′ to [BP]dG6 and proceeding toward dG12 located at the other end of the helix (solid line). The diagonal cross peaks corresponding to the imino protons of dT4, dT20, dT8, dT14, dG22, dG21, dG12, dG13, dG16, and dG18 are labeled. The cross peak labeled "a" designates a dG16(NH1) exchange cross peak. (B) NOE connectivities between the imino protons (10.3−14.1 ppm) and the nucleic acid base and amino protons and the benzo[*a*]pyrenyl protons (4.3−8.7 ppm) are designated for the d(A3-T4-C5-[BP]G6-C7-T8-A9)·d(T14-A15-G16-C17-G18-A19-T20) segment of the (−)-*cis-anti*-[BP]dG·dC 11-mer duplex. The cross peaks A−C designate thymidine imino to adenosine H2 protons connectivities across the pair and are assigned as follows: A, dT4(NH3)-dA19(H2) and dT20(NH3)-dA3-(H2); B, dT8(NH3)-dA15(H2); C, dT14(NH3)-dA9(H2). The exchange cross peak between the [BP]dG6 imino proton and H_2O is designated D. The cross peaks E,E′ and F,F′ designate guanosine imino to cytidine amino proton connectivities across the pair and are assigned as follows: E,E′, dG16(NH1)-dC7(NH_2-4b,e); F,F′, dG18(NH1)-dC5(NH_2-4b,e). The cross peaks b−d designate additional connectivities between the imino protons of dG16 and dG18 to surrounding nucleic acid protons and are assigned as follows: b, dG16(NH1)-dC7(H5); c, dG18(NH1)-dC5(H5); d, dG18(NH1)-dA19(H2). The cross peaks 1−10 between nucleic acid and BP protons are assigned as followed: 1, dG16(NH1)-BP(H9); 2, dG16-(NH1)-BP(H10); 3, dG16(NH1)-BP(H5); 4, dG16(NH1)-BP(H3) and/or BP(H4); 5, dG16(NH1)-BP(H6); 6, dG16(NH1)-BP(H11); 7, dG18(NH1)-BP(H3) and/or BP(H4); 8, dG18(NH1)-BP(H12); 9, dG18(NH1)-BP(H2); 10, dG18(NH1)-BP(H1).

Table 1: Proton Chemical Shifts of the d(T4-C5-[BP]G6-C7-T8)·d(A15-G16-C17-G18-A19) Segment of the (−)-*cis-anti*-[BP]dG·dC 11-mer Duplex in Aqueous Buffer

Exchangeable Proton Chemical Shifts (ppm) at 1 °C			
	G(NH1)/T(NH3)	G(NH_2-2)	C(NH_2-4)
dT4·dA19	13.60		
dC5·dG18	10.94		6.64,[b] 5.52[c]
[BP]dG6·dC17	11.50	8.62[a]	
dC7·dG16	10.98		6.77,[b] 6.62[c]
dT8·dA15	13.58		

Nonexchangeable Proton Chemical Shifts (ppm) at 10 °C						
	H8/H6	H2/H5/CH_3	H1′	H2′,H2″	H3′	H4′
dT4	6.86	1.09	5.69	1.39, 1.88	4.66	4.01
dC5	6.04	4.41	5.47	0.83, 1.63	4.27	4.14
[BP]dG6	8.23		6.74	3.23, 2.81	5.33	4.79
dC7	7.75	5.74	4.47[a]	2.01,[a] 2.13[a]	4.93[a]	4.14[a]
dT8	7.44	1.55	5.62	2.08, 2.47	4.75	4.09
dA15	8.22	6.67	5.87	2.75, 4.37	5.05	4.37
dG16	7.86		5.93	2.56, 2.75	5.06	4.48
dC17	7.97	5.92	6.30	2.35, 2.65	4.86	4.48
dG18	8.15		5.50	2.71, 2.77	5.00	4.42
dA19	8.39	7.72	6.29	2.77, 2.92	5.07	4.50

[a] Tentative assignment. [b] Hydrogen-bonded amino proton. [c] Exposed amino proton.

°C using standard nucleic acid assignment procedures (Hare et al., 1983).

An expanded plot of the 300 ms mixing time NOESY spectrum correlating the purine H8 and pyrimidine H6 protons (5.9−8.7 ppm) to the sugar H1′ protons (4.2−6.8 ppm) of the (−)-*cis-anti*-[BP]dG·dC 11-mer duplex in D_2O buffer, pH 7.0, at 10 °C is shown in Figure 3. The base to sugar H1′ connectivities along the modified strand are traced from dT4 to dT8 (solid line, Figure 3), with a break occurring at the dC5-[BP]dG6 step (box, Figure 3), and from dA15 to dA19 along the complementary strand (dashed line, Figure 2) with a break occurring at the dC17-dG18 step. However, a weak cross peak between dC17(H1′) and dG18(H8) is detected in the 150 ms mixing time NOESY of the duplex adduct in H_2O buffer at 1 °C (peak B, Supporting Information, Figure S1). These base and sugar H1′ sugar assignments have been confirmed by cross-checks in other regions of the NOESY plot which have also yielded a complete set of sugar H2′, H2″, H3′, and H4′ proton assignments. The only exceptions are the sugar proton assignments of dC7, which are tentative at this time. Resonances involving the base and sugar protons of this residue are broad, and hence their NOE and coupling connectivities are weak or missing. The chemical shifts of the nonexchangeable nucleic acid protons are listed for the d(T4-C5-[BP]G6-C7-T8)·d(A15-G16-C17-G18-A19) segment of the (−)-*cis-anti*-[BP]dG·dC 11-mer duplex in Table 1 and for the entire adduct duplex in Supporting Information Table S2.

Both the exchangeable and nonexchangeable proton chemical shift changes on proceeding from the control duplex to the adduct duplex for the central d(T4-C5-[BP]G6-C7-T8)·d(A15-G16-C17-G18-A19) segment are summarized in Supporting Information Table S3.

Nonexchangeable Benzo[a]pyrenyl Protons. The nonexchangeable benzo[*a*]pyrenyl protons were assigned from an analysis of the through-space NOE patterns (Figure 3) and through-bond coupling connectivities in the (−)-*cis-anti*-[BP]-dG·dC 11-mer duplex. These proton chemical shifts are plotted schematically in Figure 4 (dark gray circles) and are tabulated in the caption of Figure 4. The (−)-*cis-anti*-[BP]-

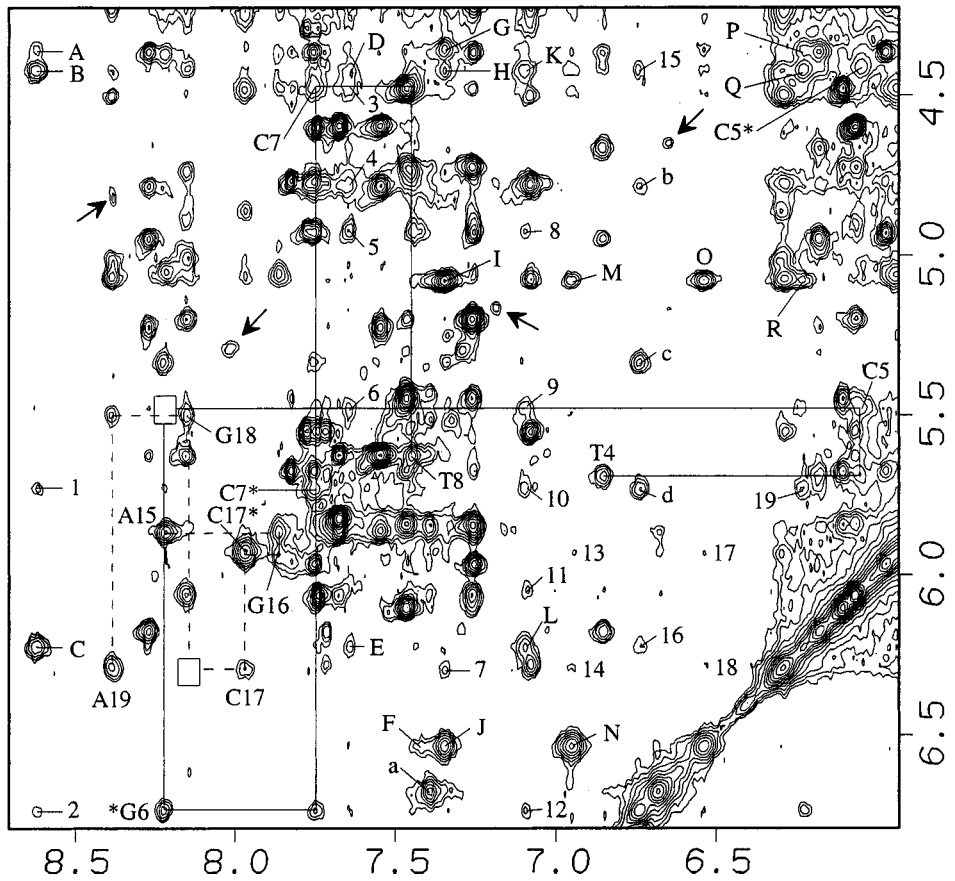

FIGURE 3: Expanded NOESY (300 ms mixing time) contour plot of the (−)-*cis-anti*-[BP]dG·dC 11-mer duplex in D_2O buffer at 10 °C establishing distance connectivities between the base (purine H8 and pyrimidine H6) protons (5.9−8.7 ppm) and the sugar H1′ and cytosine H5 protons (4.2−6.8 ppm) for the d(T4-C5-[BP]G6-C7-T8)·d(A15-G16-C17-G18-A19) segment. The NOE connectivities between the base and their own and 5′-flanking sugar H1′ protons are traced from dT4 to dT8 on the modified strand (solid line), with the break in connectivity at the dC5(H1′) to [BP]dG6(H8) step boxed, and from dA15 to dA19 on the unmodified complementary strand (dashed line), with the break in connectivity at the dC17(H1′) to dG18(H8) step boxed. The cross peaks between cytosine H5 and H6 protons are designated by an asterisk. The cross peaks labeled A−R identify NOEs between benzo[*a*]pyrenyl protons and are assigned as follows: A, BP(H11)-BP(H8); B, BP(H11)-BP(H9); C, BP(H11)-BP(H10); D, BP(H1)-BP(H9); E, BP(H1)-BP(H10); F, BP(H2)-BP(H5); G, BP(H6)-BP(H8); H, BP(H6)-BP(H9); I, BP(H6)-BP(H7); J, BP(H6)-BP(H5); K, BP(H12)-BP(H9); L, BP(H12)-BP(H10); M, BP(H3) and/or BP(H4)-BP(H8); N, BP(H3) and/or BP(H4)-BP(H9); O, BP(H5)-BP(H7); P, BP(H10)-BP(H8); Q, BP(H10)-BP(H9); R, BP(H10)-BP(H7). The cross peaks numbered 1−19 identify BP-DNA NOEs and are assigned as follows: 1, BP(H11)-dC7(H5); 2, BP(H11)-[BP]dG6(H1′); 3, BP(H1)-dC7(H1′); 4, BP(H1)-[BP]dG6(H4′); 5, BP(H1)-dC7(H3′); 6, BP(H1)-dC5(H1′); 7, BP(H6)-dC17(H1′); 8, BP(H12)-dC7(H3′); 9, BP(H12)-dC5(H1′); 10, BP(H12)-dC7(H5); 11, BP(H12)-dC5(H6); 12, BP(H12)-[BP]dG6(H1′); 13, BP(H3) and/or BP(H4)-dC17(H5); 14, BP(H3) and/or BP(H4)-dC17(H1′); 15, BP(H9)-[BP]dG6(H1′); 16, BP(H10)-[BP]dG6(H1′); 17, BP(H5)-dC17(H5); 18, BP(H5)-dC17(H1′); 19, BP(H10)-dC7(H5). Examples of exchange cross peaks in the spectrum are indicated by arrows.

dG benzo[*a*]pyrenyl proton chemical shift values are compared to the corresponding values in the stereomeric (+)-*trans-anti*-[BP]dG·dC (black squares; Cosman et al., 1992), (−)-*trans-anti*-[BP]dG·dC (open triangles; de los Santos et al., 1992), and (+)-*cis-anti*-[BP]dG·dC (light gray diamonds; Cosman et al., 1993a) 11-mer duplexes in Figure 4. The stereochemical orientation of the benzylic ring hydroxyl and dG(N^2) substituents of these four diastereomers are shown at the top of Figure 4. The BP aromatic pyrenyl ring protons resonate between 8.0 and 8.5 ppm in the (+)- and (−)-*trans*-[BP]dG·dC adduct duplexes, in which the pyrenyl ring system is located in the minor grooves of the adduct duplexes and exposed to solvent. In contrast, they resonate upfield between 6.5 and 8.0 ppm in the (+)-*cis-anti*-[BP]dG·dC adduct duplex, in which the pyrenyl ring intercalates between dC5·dG18 and dC7·dG16 base pairs. Similarly, the aromatic pyrenyl ring protons in the (−)-*cis-anti*-[BP]dG·dC adduct duplex resonate upfield between 6.5 and 8.0 ppm. The pyrenyl ring protons that exhibit the largest ring current effects are BP(H5) followed by BP(H3), BP(H4), and BP(H12).

BP-DNA NOEs in the (−)-cis-anti-[BP]dG·dC 11-mer Duplex. A set of 35 BP-DNA NOE cross peaks, including 14 involving exchangeable protons, have been identified in the NOESY spectra of the (−)-*cis-anti*-[BP]dG·dC adduct duplex (Table 2). Most of these BP-DNA NOE cross peaks are labeled by numbers in the expanded NOESY plots of the exchangeable protons in H_2O solution (Figures 2B and S1) and nonexchangeable protons in D_2O solution (Figure 3). The BP-DNA cross peak assignments are listed in the captions of Figures 2, 3, and S1.

The distribution of proton distance restraints is such that they are restricted to NOEs between the protons of BP and the d(C5-[BP]G6-C7)·d(G16-C17-G18) segment of the adduct duplex (Table 2). Most of the NOE cross peaks involving benzo[*a*]pyrenyl and DNA protons exhibit weak intensities, reflecting conformational perturbations associated with the alignment of (−)-*cis-anti*-[BP]dG6 and dC17 at the lesion site. Two possible explanations for the observation of a weak NOE cross peak are that either the distance between the two protons is long (4.0−5.5 Å range), or the distance between the two protons is close but one or both of

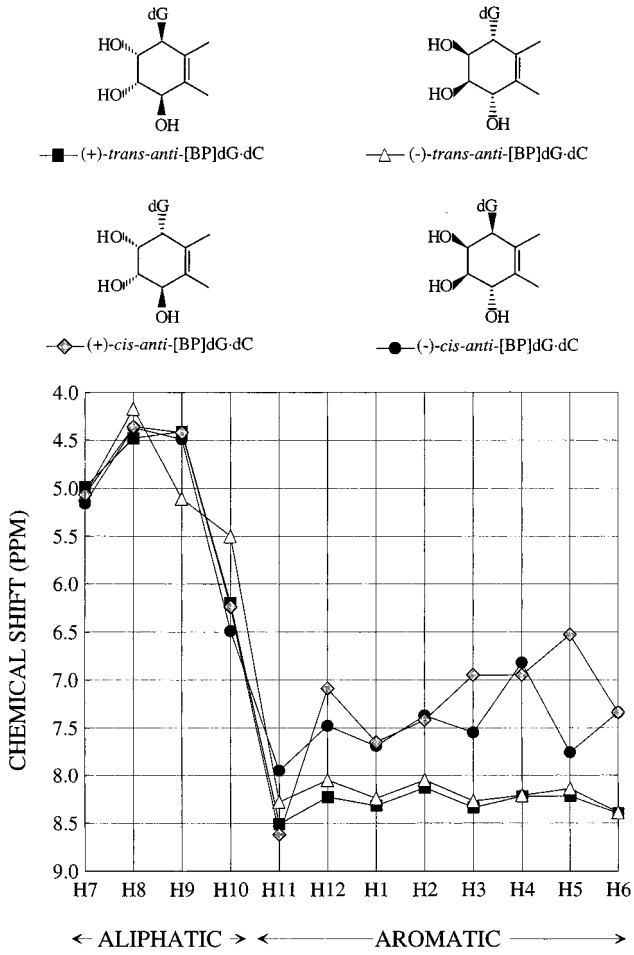

FIGURE 4: Plot comparing the benzo[*a*]pyrenyl ring proton chemical shifts in the stereomeric (+)-*trans*-, (−)-*trans*-, (+)-*cis*-, and (−)-*cis-anti*-[BP]dG·dC 11-mer duplexes. The stereochemical orientations of the benzylic hydroxyl and [BP]dG6(N^2) substituents are shown above the plot. The chemical shifts values in ppm for the BP protons in the (−)-*cis-anti*-[BP]dG·dC 11-mer duplex are as follows: BP(H7), 5.07; BP(H8), 4.36; BP(H9), 4.42; BP(H10), 6.24; BP(H11), 8.62; BP(H12), 7.09; BP(H1), 7.65; BP(H2), 7.42; BP-(H3), 6.95; BP(H4), 6.95; BP(H5), 6.53; BP(H6), 7.34.

Table 2: Comparison of Experimental Distance Restraints with Those Observed for the NMR Energy-Minimized Structure of the (−)-*cis-anti*-[BP]dG·dC 11-mer Duplex

	interproton distances (Å)	
	experimental bounds	observed
exchangeable protons		
dC7(NH-4b)-BP(H9)[a]	2.2−6.0	3.20
dC7(NH-4b)-BP(H11)[a]	2.2−6.0	4.34
dC7(NH-4e)-BP(H9)[a]	2.2−6.0	2.49
dC7(NH-4e)-BP(H11)[a]	2.2−6.0	3.95
dG16(NH1)-BP(H3) and/or BP(H4)	4.0−6.0	5.47, 4.74
dG16(NH1)-BP(H5)	4.0−6.0	4.25
dG16(NH1)-BP(H6)	4.0−6.0	4.34
dG16(NH1)-BP(H9)	4.0−6.0	5.47
dG16(NH1)-BP(H10)	4.0−6.0	4.88
dG16(NH1)-BP(H11)	4.0−6.0	4.97
dG18(NH1)-BP(H1)	3.0−5.0	3.89
dG18(NH1)-BP(H2)	3.0−5.0	4.55
dG18(NH1)-BP(H3) and/or BP(H4)	3.0−5.0	4.73, 5.13
dG18(NH1)-BP(H12)	3.0−5.0	3.90
nonexchangeable protons		
dC5(H1′)-BP(H1)	3.5−5.5	5.55
dC5(H1′)-BP(H12)	3.5−5.5	4.53
dC5(H6)-BP(H11)	3.5−5.5	5.03
dC5(H6)-BP(H12)	4.0−6.0	5.84
[BP]dG6(H1′)-BP(H9)	4.0−6.0	5.87
[BP]dG6(H1′)-BP(H10)	3.5−5.5	4.18
[BP]dG6(H1′)-BP(H11)	3.5−5.5	3.63
[BP]dG6(H1′)-BP(H12)	3.5−5.5	4.46
[BP]dG6(H4′)-BP(H1)	3.5−5.5	4.82
dC7(H1′)-BP(H1)[a]	2.2−6.0	2.36
dC7(H3′)-BP(H1)[a]	2.2−6.0	6.14
dC7(H3′)-BP(H12)[a]	2.2−6.0	6.04
dC7(H5)-BP(H10)[a]	2.2−6.0	3.01
dC7(H5)-BP(H11)[a]	2.2−6.0	3.25
dC7(H5)-BP(H12)[a]	2.2−6.0	4.38
dC7(H6)-BP(H11)[a]	2.2−6.0	3.67
dC17(H1′)-BP(H3) and/or BP(H4)[a]	2.2−6.0	4.42, 2.32
dC17(H1′)-BP(H5)[a]	2.2−6.0	2.90
dC17(H1′)-BP(H6)[a]	2.2−6.0	5.24
dC17(H5)-BP(H3) and/or BP(H4)[a]	2.2−6.0	9.06, 6.73
dC17(H5)-BP(H5)[a]	2.2−6.0	5.43

[a] The line widths for the base and sugar resonances of dC7 and dC17 are large; therefore, wide experimental bounds were given for distances involving these protons of 2.2−6.0 Å.

the line widths of these resonances are broad. Since the line widths of the base and sugar resonances of dC7 and dC17 are large (Figure 1B), the upper and lower bounds of the NMR-derived BP-DNA distance restraints involving protons of these two residues were assigned wide bounds (2.2−6.0 Å, Table 2).

The distribution of the NOEs between benzo[*a*]pyrenyl protons and exchangeable nucleic acid protons involve exclusively the imino protons of dG16 and dG18 and the amino protons of dC7 in the d(C5-[BP]G6-C7)·d(G16-C17-G18) segment of the adduct duplex (Table 2). The combined pattern of specific BP-DNA NOEs (Table 2), upfield chemical shift differences between the control and adduct duplex for the amino and imino protons of the dC5·dG18 and dC7·dG16 base pairs (Table S3), and upfield pyrenyl proton chemical shifts (Figure 4) establish unambiguously that the BP ring intercalates between intact dC5·dG18 and dC7·dG16 base pairs.

We observe distinct trends in the patterns of the nonexchangeable BP-DNA NOEs that permit the alignment of the different edges of the intercalated BP ring relative to the modified and unmodified strands of the adduct duplex. These intermolecular NOEs explicitly establish that the long axis of the intercalated benzo[*a*]pyrenyl moiety is normal to the long axis of the flanking base pairs and spans both grooves of the helix.

The observed downfield chemical shifts of the base and sugar protons of the [BP]dG6 residue (Table S3), the disruption of the hydrogen-bonding alignment of the [BP]-dG6·dC17 base pair (Figure 2B), and the rapid exchange of the imino proton of [BP]dG6 with solvent (peak D, Figure 2B) establishes that the modified deoxyguanosine must be looped out of the helix.

Molecular Mechanics Computations. The conformational search strategy employed in the molecular mechanics program DUPLEX began with a B-DNA (Arnott et al., 1976) central 5-mer d(T4-C5-[BP]G6-C7-T8)·d(A15-G16-C17-G18-A19) segment of the (−)-*cis-anti*-[BP]dG·dC 11-mer duplex. In these trials the DUPLEX hydrogen-bond penalty function (Hingerty et al., 1989) for Watson−Crick base pairing was utilized at all base pairs except at the lesion site, since the NMR data excluded the pairing of the [BP]dG6 and dC17 residues. The NMR-derived upper and lower bound distance restraints involving BP-DNA interactions (Table 2) were included. In addition, DNA−DNA distance

restraints for the pentanucleotide segments of both strands centered about the lesion site (Table S5) were also included in the computations. For these latter restraints, strong, medium, and weak cross peak intensities were given bounds of 2.5−4.0 Å, 3.0−5.0 Å, and 4.0−6.0 Å, respectively. We did not restrain those cross peaks whose intensities are listed as absent in Table S5. The BP-DNA orientation space was then searched with 16 energy minimization trials in which the linkage torsion angles α' ([BP]dG6(N^1)-[BP]dG6(C^2)-[BP]dG6(N^2)-BP(C^{10})) and β' ([BP]dG6(C^2)-[BP]dG6(N^2)-BP(C^{10})-BP(C^9)) were each started at 0°, 90°, 180°, and 270° in all combinations. Searching orientation space at 90° intervals of α' and β' is a robust procedure for locating all the important potential energy wells because our minimization protocol permits torsion angle variations of up to 100° in each minimization step (Hingerty et al., 1989). Consequently, energy minima in each quadrant of α' and β' are accessible, and the reduced variable domain of torsion angle space greatly enhances the likelihood of finding the important structures.

Of the 16 structures computed, three structures exhibited the lowest energies and the best fit to the NMR data. These three conformers were identified as being in the family of structures in which the pyrenyl ring of the (−)-*cis-anti*-[BP]-dG adduct intercalates between intact dC5·dG18 and dC7·dG16 base pairs and the modified deoxyguanosine and covalently attached benzylic ring are located in the major groove. A view looking into the major groove and normal to the helical axis of the central pentanucleotide duplex segment showing the superposition of these three structures is shown in Figure 5A, while a view looking down the helical axis of the central d(C5-[BP]G6-C7)·d(G16-C17-G18) trimer segment showing the overlap geometry of the BP ring and flanking dC5·dG18 and dC7·dG16 pairs is shown in Figure 5B.

The pairwise RMS deviation values of the d(T4-C5-[BP]-G6-C7-T8)·d(A15-G16-C17-G18-A19) segment of the three low energy structures are 1.41, 1.55, and 2.20 Å, indicating that these three structures manifest some differences in structural details. However, each of these three restrained pentamers exhibit good agreement with the NMR data. Consequently, each of the three conformers was embedded into an energy-minimized B-form 11-mer and reminimized with all restraints. Subsequently, the hydrogen-bond penalty function and the distance restraints were released with energy minimization in one step, yielding three final unrestrained structures. One of these three unrestrained 11-mer structures had the lowest energy and the best fit to the NMR data (Table 2).

Solution Structure. A view normal to the helix axis and looking into the major groove of the d(T4-C5-[BP]G6-C7-T8)·d(A15-G16-C17-G18-A19) segment of the NMR energy-minimized structure of the (−)-*cis-anti*-[BP]dG·dC 11-mer duplex is shown in Figure 6A. The benzo[*a*]pyrenyl ring which is covalently linked to the minor groove N^2 of dG6 intercalates between intact dC5·dG18 and dC7·dG16 base pairs and in the process displaces the modified deoxyguanosine residue into the major groove (Figure 6A). The plane of the [BP]dG6 aromatic purine ring is directed toward the 5′-end of the modified strand, is tilted ∼132° relative to the long axis of the planar pyrenyl ring of BP, and stacks over the major groove edge of the 5′-side dC5 residue. The partner dC17 residue is also displaced into the major groove.

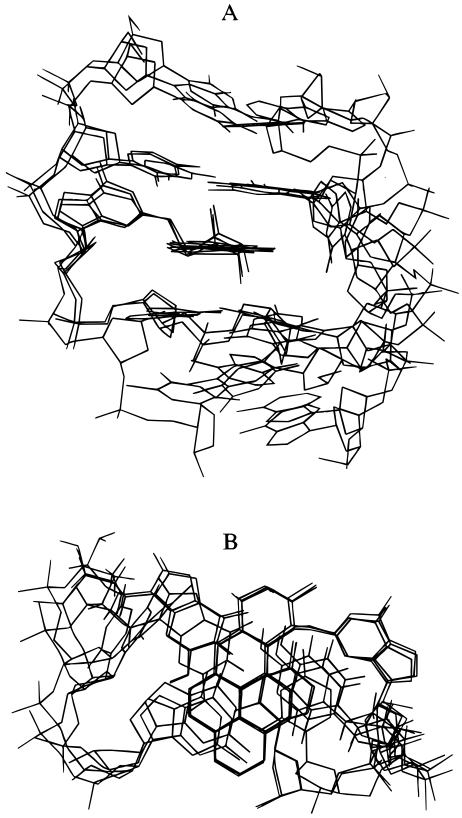

FIGURE 5: Superposition of the three d(T4-C5-[BP]G6-C7-T8)·d(A15-G16-C17-G18-A19) central 5 base pair segments that best fit the NMR data of the (−)-*cis-anti*-[BP]dG·dC 11-mer duplex obtained from the 16 trials to search conformational space using NMR restraints (Table 2) and the program DUPLEX. (A) View looking into the major groove and normal to the helix axis of the central 5-mer segments and (B) view looking down the helix axis of the central d(C5-[BP]G6-C7)·d(G16-C17-G18) segment.

A view looking down the helix axis of the d(C5-[BP]G6-C7)·d(G16-C17-G18) segment of the NMR energy-minimized structure of the (−)-*cis-anti*-[BP]dG·dC 11-mer duplex emphasizing the overlap geometry of the BP moiety and the flanking dG·dC base pairs is shown in Figure 6B. The long axis of the intercalated benzo[*a*]pyrenyl ring is normal to the long axis of the flanking dC5·dG18 and dC7·dG16 base pairs with its benzylic ring positioned in the major groove and the farthest aromatic ring on the pyrenyl ring extending to, but not into, the minor groove.

The benzylic ring of BP is in a distorted half-chair conformation with BP(H7), BP(H8), and BP(H10) in pseudoequatorial orientations and BP(H9) protons in a pseudoaxial orientations. The carcinogen−base linkage site for the [BP]dG6 residue is defined by the angles α' ([BP]dG6(N^1)-[BP]dG6(C^2)-[BP]dG6(N^2)-BP(C^{10})) = 135° and β' ([BP]-dG6(C^2)-[BP]dG6(N^2)-BP(C^{10})-BP(C^9)) = 268° in the NMR energy-minimized structure of the (−)-*cis-anti*-[BP]dG·dC 11-mer duplex.

The χ glycosidic torsion angle values, sugar pucker pseudorotation parameters **P** (Altona & Sundaralingnam, 1972), and backbone torsion angles for the d(T4-C5-[BP]-G6-C7-T8)·d(A15-G16-C17-G18-A19) segment of the NMR energy-minimized structure of the (−)-*cis-anti*-[BP]dG·dC 11-mer duplex are listed in Supporting Information Table S4. A number of values differ from those that are typical for B-DNA. However, the less prevalent conformational

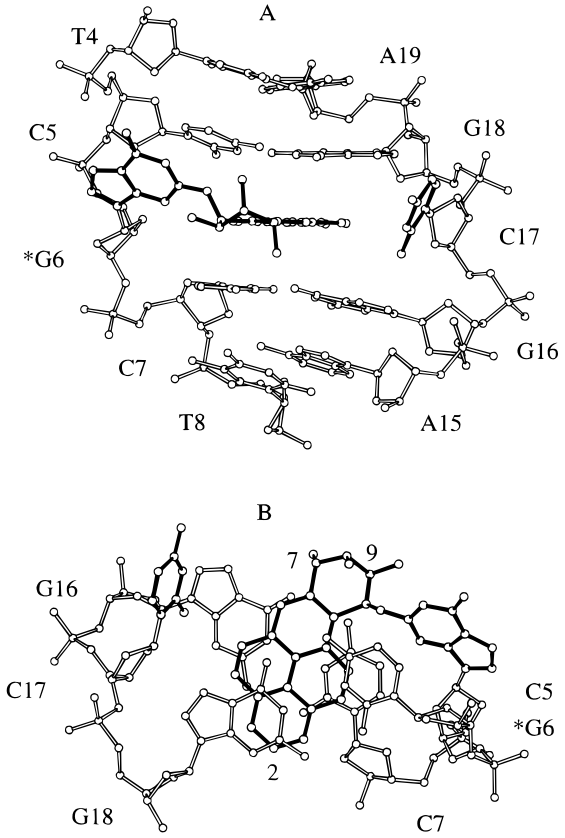

FIGURE 6: (A) View looking into the major groove and normal to the helix axis for the d(T4-C5-[BP]G6-C7-T8)·d(A15-G16-C17-G18-A19) segment in the solution structure of the (−)-*cis-anti*-[BP]dG·dC 11-mer duplex. The BP ring system is shown in darkened bonds and is intercalated between the dC5·dG18 and dC7·dG16 base pairs. The modified [BP]dG6 and dC17 bases, shown in darkened bonds, are displaced into the major groove. The plane of the [BP]dG6 base is tilted by ∼132° relative to the helix axis. The [BP]dG6 base is directed toward its 5′-neighbor dC5 in the sequence. (B) View looking down the helix axis for the d(C5-[BP]G6-C7)·d(G16-C17-G18) segment in the solution structure of the (−)-*cis-anti*-[BP]dG·dC 11-mer duplex. Note that the benzylic ring is positioned in the major groove, while the pyrenyl ring stacks over the Watson−Crick hydrogen bonding regions of the flanking dC5·dG18 and dC7·dG16 base pairs. The major groove edges of the dC5 base and sugar rings are positioned over the plane of the displaced [BP]dG6 residue. Figures were prepared using Molscript V1.1 (Kraulis, 1991).

domains noted here have all been observed in B-DNA crystals (Berman et al., 1992) and are within the normal range of B-DNA flexibility.

The dT4·dA15 and dC5·dG18 base pairs located 5′ to the lesion site and the 3′-side dC7·dG16 and dT8·dA15 pairs in the d(T4-C5-[BP]G6-C7-T8)·d(A15-G16-C17-G18-A19) segment are buckled and propeller twisted in the NMR energy-minimized structure of the (−)-*cis-anti*-[BP]dG·dC 11-mer duplex (Figure 6A). The base pair buckle and propeller twist values, and the twist angles and rise distances between flanking bases for the entire adduct duplex were computed using the method developed by Babcock et al. (1993) and are plotted graphically in Supporting Information Figure 2. The double helix at the dC5·dG18 to dC7·dG16 two-base pair step unwinds by 25°, indicating an average unwinding angle of the helix between the displaced [BP]dG6·dC17 and flanking dG·dC pairs of 12−13°. It is interesting to note that the distortion to the adduct duplex in the NMR energy-minimized structure of the of the (−)-*cis-anti*-[BP]dG·dC adduct duplex extends farther than two base pairs on either side of the lesion site.

DISCUSSION

Spectral Quality and Conformational Equilibrium. Our structural studies are based on NMR spectra of the (−)-*cis-anti*-[BP]dG·dC 11-mer duplex at low temperature (1 °C in H_2O buffer and 10 °C in D_2O buffer) since these were optimal conditions for targeting the major conformation which was in slow exchange with a minor conformation in this temperature range. The line widths for both exchangeable (Figure 1A) and nonexchangeable (Figure 1B) proton resonances of the d(T4-C5-[BP]G6-dC7-T8)·d(A15-G16-C17-G18-A19) segment broaden upon formation of the (−)-*cis-anti*-[BP]dG adduct positioned opposite dC at the duplex level. The observed broadening was manifested both in the increased line widths of individual protons in the vicinity of the lesion site and also in the presence of a broad envelope as seen in the base and sugar H1′ nonexchangeable proton spectral region in Figure 1b. These large proton resonance line widths, in turn, result in the observation of predominantly weak NOEs between the BP protons and neighboring nucleic acid protons (Table 2 and Figures 2, 3, and S1) making it difficult to accurately gauge the intensity of the NOE cross peaks used in determining the NMR-derived distance bounds. Moreover, the broader line widths of the resonances in the central 5-mer segment of the adduct duplex preclude obtaining coupling constant information for the sugar pucker conformations of these residues, as well as for the benzylic ring pucker conformation of the BP moiety. The difficulty of analyzing the NMR spectra of the (−)-*cis-anti*-[BP]dG·dC 11-mer duplex is further compounded by the poor spectral resolution of many of the resonances involving protons located in the central 5-mer segment and by the presence of numerous exchange cross peaks between a major and a minor conformation (examples indicated by peak "a" in Figure 2A and by arrows in Figure 3). However, despite broad and overlapped resonances, the analysis of the NOESY and TOCSY data sets have permitted the assignments of base and sugar protons of the major conformer, with the exception of the sugar H1′, H2′, H2″, and H4′ protons of dC7, which remain tentative at this time (Table 1). Not only were the line widths of the base and sugar proton resonances of dC7 very large, but the base H6 proton of dC7 overlaps with the base H8 protons of dG13 and dG22.

The observation of exchange cross peaks in the NOESY spectra of the (−)-*cis-anti*-[BP]dG·dC 11-mer duplex establish a slow equilibrium between the major conformer which is the focus of this study and a minor conformer which could not be characterized in any detail. Conformational exchange was similarly observed for the (+)-*cis-anti*-[BP]-dG·dC 11-mer duplex in the same duplex sequence (Cosman et al., 1993a) and for the (+)-*trans-anti*-[BP]dG·dC adduct when the 5′-flanking base pair was dA·dT instead of dG·dC (Fountain & Krugh, 1995).

Intercalation Site. The NMR energy-minimized structure of the (−)-*cis-anti*-[BP]dG·dC 11-mer duplex must not only satisfy the distance restraints but also be consistent with the observed chemical shift changes associated with intercalation of the pyrenyl ring into the helix. Let us start by evaluating whether the BP-DNA NOE distance restraints listed in Table 2 are satisfied by the structure shown in Figure 6. The

intercalation of the BP ring into the helix between intact dC5·dG18 and dC7·dG16 pairs with accompanying displacement of the modified base pair (Figure 6A) is supported by the observation of several NOEs between the imino protons of dG16 and dG18 and the benzo[*a*]pyrenyl protons located on different edges of the planar pyrenyl ring (Figure 2B and Table 2) although the dG16 and dG18 residues are not adjacent to each other in the d(C5-[BP]G6-C7)·d(G16-C17-G18) sequence. The orientation of the benzo[*a*]pyrenyl $C^9-C^{10}-C^{11}-C^{12}$ bay region containing edge toward the modified strand in the NMR energy-minimized structure of the adduct duplex (Figure 6B) is supported by the observation of NOEs between the H9, H10, H11, and H12 protons of BP and the base and sugar protons of dC5, [BP]dG6, and dC7 (Figure 3 and Table 2). The opposite side $C^4-C^5-C^6$ edge of the BP ring is directed toward the unmodified strand (Figure 6B), and this result is upheld by the NOEs observed between the H4, H5, and H6 protons of BP and the H1′ and H5 protons of dC17 (Figure 3 and Table 2). The location of the covalently attached benzylic ring in the major groove of the helix (Figure 6) is supported by the presence of NOEs between the aliphatic BP(H9) and BP(H10) protons and the H5, H6, and amino protons of dC7 (Figures 3 and S1 and Table 2). The aromatic pyrenyl ring located farthest away from the benzylic ring extends to the minor groove edge of the helix (Figure 6B) as evidenced by the NOEs between the BP(H1) proton and the H1′ protons of dC5 and dC7 (Figure 3 and Table 2).

Let us next evaluate whether the observed proton chemical shift patterns (Table S4) can be qualitatively explained by the overlap geometries between the benzo[*a*]pyrenyl ring and flanking dG·dC base pairs in the structure. The pyrenyl ring BP(H1), BP(H2), BP(H3), BP(H4), BP(H5), BP(H6), BP(H11), and BP(H12) protons sandwiched between flanking dG·dC base pairs (Figure 6B) should experience upfield ring shifts. The largest shifts would be predicted and are observed experimentally for the BP(H3), BP(H4), and BP(H5) protons (Figure 4) which are directly stacking over the aromatic purine rings of dG16 and dG18. Since the benzylic ring BP(H7), BP(H8), BP(H9), and BP(H10) protons located in the major groove of the helix do not stack with adjacent nucleic acid bases, they exhibit chemical shifts that are similar to the corresponding values observed for the (+)-*trans*-, (−)-*trans*-, and (+)-*cis-anti*-[BP]dG6 stereoisomers (Figure 4) in the same duplex sequence context.

The plane of the intercalated pyrenyl ring is parallel to the planes of the flanking dG·dC base pairs, with the long axis of the BP ring normal to the long axes of the dG·dC base pairs and the aromatic pyrenyl ring centered directly over the Watson−Crick hydrogen bonding edges of the dC5·dG18 and dC7·dG16 base pairs. Thus, relative to the corresponding values in the control duplex, large upfield chemical shifts would be expected and are observed for the imino and amino protons of the dC5·dG18 and dC7·dG16 base pairs, with the exception of the exposed amino proton of dC7 (Table S3). This proton stacks over the benzylic ring rather than the aromatic pyrenyl ring of BP and can potentially form a weak hydrogen bond to the BP(OH-8) oxygen in the NMR energy-minimized structure of the (−)-*cis-anti*-[BP]dG·dC 11-mer duplex [the distance between dC7(NH_2-4e) hydrogen and BP(OH-8) oxygen is 2.92 Å].

Effects of [BP]dG6 and dC17 Displacement into the Major Groove on DNA Structure. Both the deoxyguanosine ring of [BP]dG6 and the deoxycytidine ring of dC17 are displaced into the major groove resulting in a loss of stacking interactions between the modified base pair and the flanking dG·dC base pairs. Hence, the usual connectivity found in unperturbed B-DNA helices between the imino protons of deoxyguanosines located in adjacent base pairs would be expected to be disrupted, and this loss of connectivity is supported experimentally by the absence of NOE cross peaks between the imino proton of [BP]dG6 and the imino protons of both its 3′-side dG16 and 5′-side dG18 neighbors (Figure 2A). In addition, the imino proton of [BP]dG6 should shift upfield since it no longer participates in hydrogen-bonding interactions with its partner dC17, while the sugar protons and the guanine H8 and cytosine H5 and H6 base protons of [BP]dG6 and dC17 should experience large downfield shifts, relative to their corresponding values in the control duplex in which the dG6·dC17 pair is hydrogen-bonded and stacked within the helix. We observe these expected chemical shift differences experimentally (Table S3), in agreement with the structure of the adduct duplex (Figure 6). The deoxyguanosine ring is directed toward the 5′-end of the modified strand with its plane at ∼132° to the helix axis and stacked over the major groove edge of dC5 in the structure (Figure 6). The large upfield chemical shifts observed for the major groove H2′, H5, and H6 protons of dC5 must reflect stacking of these protons over the deoxyguanosine ring of [BP]dG6 in the structure.

The positions of the dC7 and dC17 residues are the least defined regions in the NMR energy-minimized structure of the (−)-*cis-anti*-[BP]dG·dC 11-mer duplex. The line widths of the base and sugar resonances of dC7 and dC17 are large indicating that these two residues experience a high degree of conformational heterogeneity. The chemical shifts of the base and sugar protons of dC7 are shifted downfield compared to their corresponding values in the control duplex, with the exception of dC7(H1′) which is shifted upfield by −1.36 ppm (Table S3). This proton is partially stacked over the edge of the pyrenyl ring in the structure (Figure 6). The remaining downfield shifts of the protons belonging to these two residues can be rationalized by the looping out of the dC17 residue out of the helix into the major groove and by the loss of stacking interactions between the dC7 base and the displaced [BP]dG6 base. In addition, the high degree of conformational heterogeneity of the dC7 residue extends to its dG16 partner. The line widths of the proton resonances of dG16 are also large, and we observe an exchange cross peak for the imino proton of dG16 in the 150 ms mixing time NOESY spectrum of the adduct duplex in H_2O solution (peak a, Figure 2A). Thus, the dC7·dG16 base pair located to the 3′ side of the lesion site exhibits a high degree of conformational heterogeneity.

The displacement of both [BP]dG6 and dC17 into the same groove appears to produce extensive helical distortions in the NMR energy-minimized central pentamer segment of the adduct duplex as evidenced by the unusual glycosidic and backbone torsion angles and sugar pseudorotation angles for the residues located in this segment (Table S4). Similar long-range helical distortions have been previously reported for the X-ray crystal structure of the noncovalent complex between the anticancer drug daunomycin and a hexanucleotide in which the planar aromatic anthraquinone ring portion of the drug intercalates between dG·dC base pairs with its long axis perpendicular to the long axes of base pairs

(Quigley et al., 1980). In both the (−)-*cis-anti*-[BP]dG and daunomycin DNA complexes, changes in C3′−O3′ and O3′−P torsion angles ϵ and ζ are observed as well as a wide variety of sugar pucker conformations for residues extending two base pairs on either side of the intercalation site. These changes in the helical parameters in the daunomycin−DNA complex have been attributed to unwinding of the helix (Saenger, 1984). However, we must point out that, despite similarities in structural distortions, the daunomycin−DNA complex forms a classical intercalation site in which the phosphodiester backbone between the two flanking dG·dC base pairs is stretched to accommodate the drug, while intercalation of the pyrenyl ring in the (−)-*cis-anti*-[BP]dG adduct duplex is accompanied by displacement of the modified base pair into the major groove.

Nevertheless, the helical distortions found in the structure of the central d(T4-C5-[BP]G6-C7-T8)·d(A15-G16-C17-G18-A19) segment of the (−)-*cis-anti*-[BP]dG·dC 11-mer duplex are supported experimentally by the observation of unusual chemical shift and NOE patterns. Comparisons of the magnitude of adjacent residue nucleic acid NOEs in the central pentamer segment with interproton distances observed for the NMR energy-minimized structure of the (−)-*cis-anti*-[BP]dG·dC adduct duplex are listed in Supporting Information Table S5.

The distance in the NMR energy-minimized structure of the adduct duplex between the [BP]dG6(H8) and the 5′-flanking dC5(H1′) protons (5.71 Å) is in agreement with the absence of the corresponding cross peak in the 300 ms mixing time NOESY of the adduct duplex in D_2O buffer (Figure 3). The distance between the dC17(H1′) and dG18-(H8) protons is 3.51 Å, and we observe a weak cross peak in the 150 ms mixing time NOESY of the adduct duplex in H_2O buffer (Figure S1). Helical distortions are also observed farther away from the central three base pair segment surrounding the lesion site, and these long-range perturbations are supported by the observation of large upfield chemical shifts, relative to the control duplex, of the sugar H2′ and H2″ protons of dT4 and base H2 proton of dA15 (Table S3), although dT4 is located two base pairs away from the modified base in the 5′ direction, while dA15 is located two base pairs away in the 3′ direction. In addition, an unusually strong cross peak is observed between the H2 protons of dA15 and dA9 (peak a, Figure 3). This result together with the upfield shift of the dA15(H2) proton can be rationalized by the high degree of propeller twisting and buckling of the base pairs in the solution structure of the adduct duplex (Figure S2) which positions the minor groove edges of dA15 and dA9 close together [distance between dA9(H2) and dA15(H2) is 3.04 Å] and places the H2 proton of dA15 directly in-between the flanking aromatic purine rings of dG16 and dA9.

Influence of [BP]dG Adduct Stereochemistry on Structure. Comparison views normal to the helical axis with the minor groove on the left and major groove on the right of the d(T4-C5-[BP]G6-C7-T8)·d(A15-G16-C17-G18-A19) segments of the (+)-*trans*- (top left; Cosman et al., 1992), (−)-*trans*- (top right; de los Santos et al., 1992), (+)-*cis*- (bottom left; Cosman et al., 1993a), and (−)-*cis-anti*-[BP]dG (bottom right, this study) adduct duplexes are shown in Figure 7.

The covalently attached BP rings in the structures of both (+)- and (−)-*trans-anti*-[BP]dG·dC adduct duplexes are located in widened minor grooves of minimally perturbed B-DNA helices with one face of the aromatic pyrenyl ring system stacked over the sugar residues of the unmodified complementary strands. However, inversion of the stereochemistry at each of the four benzylic ring carbons of the two *trans-anti*-[BP]dG adducts (top, Figure 4) affects whether the direction of the long axis of the pyrenyl ring will point toward the 5′-end [in the structure of the (+)-*trans*-isomer, Figure 7A] or toward the 3′-end [in the structure of the (−)-*trans* isomer, Figure 7B].

The stereochemistry of the (+)-*cis-anti*-[BP]dG adduct differs from the (+)-*trans-anti*-[BP]dG isomer at a single carbon at the C^{10} binding site (top, Figure 4), and yet their adduct duplex structures are very different from one another in that the (+)-*cis-anti*-[BP]dG·dC adduct duplex adopts a base-displaced intercalation structural motif (Figure 7C), while the (+)-*trans-anti*-[BP]dG·dC isomer adopts a minor groove structural motif (Figure 7A).

The stereochemistry of the (+)-*cis-anti*-[BP]dG adduct differs from that of the (−)-*cis-anti*-[BP]dG isomer by inversion at each benzylic ring carbon (top, Figure 4), but their adduct duplexes display similar base displaced-intercalated structural features for their major conformers (Figure 7C,D). An important characteristic that both (+)- and (−)-*cis-anti*-[BP]dG·dC 11-mer duplexes share in common is the equilibrium in solution of two or more conformers, as evidenced by the presence of exchange cross peaks in the NMR spectra.

Importantly, the orientations of the intercalated BP rings in the structures of the (+)- and (−)-*cis-anti*-[BP]dG·dC adduct duplexes differ by which groove the benzylic ring resides in (Figure 7C,D). That is, the benzylic ring is located in the minor groove in the (+)-*cis-anti*-[BP]dG·dC adduct duplex, while it is positioned in the major groove in the (−)-*cis-anti*-[BP]dG·dC adduct duplex (Figure 7C,D). Thus the adduct pairs position the BP moiety oppositely, in a plane perpendicular to the helix axis. It is interesting to note that this opposite orientation of the BP moiety in the structures of the two *cis* adduct duplexes is due to a 180° flip along its long axis solely, and not along its short axis since the C^{10}−C^{11} bay region containing edge of the BP ring remains oriented toward the modified strand in both cases.

The hydrogen-bonding alignments of the modified [BP]-dG6·dC17 pair are disrupted and the deoxyguanosine and partner deoxycytosine residues displaced out of the helix and into the grooves in the structures of both (+)- and (−)-*cis-anti*-[BP]dG·dC adduct duplexes. However, the pattern of base displacement is different for each adduct duplex. Thus, the [BP]dG6 is displaced into the minor groove, and dC17 is displaced in the major groove in the structure of the (+)-*cis-anti*-[BP]dG·dC 11-mer duplex (Figure 7C), while both [BP]dG6 and dC17 are displaced into the major groove in the structure of the (−)-*cis-anti*-[BP]dG·dC 11-mer duplex (Figure 7D). The placement of both displaced residues into the same groove, as in the structure of the (−)-*cis* adduct duplex, appears to cause a greater distortion to the helix (Figure 7D). Unusual backbone torsion angles and sugar pucker conformations are computed for the modified base pair and residues located within two base pairs on either side in the NMR energy-minimized solution structure of the (−)-*cis-anti*-[BP]dG·dC 11-mer duplex.

It has long been known that the binding of *anti*-BPDE to native DNA can give rise to two different types of adduct conformations known as site I and site II; based on UV

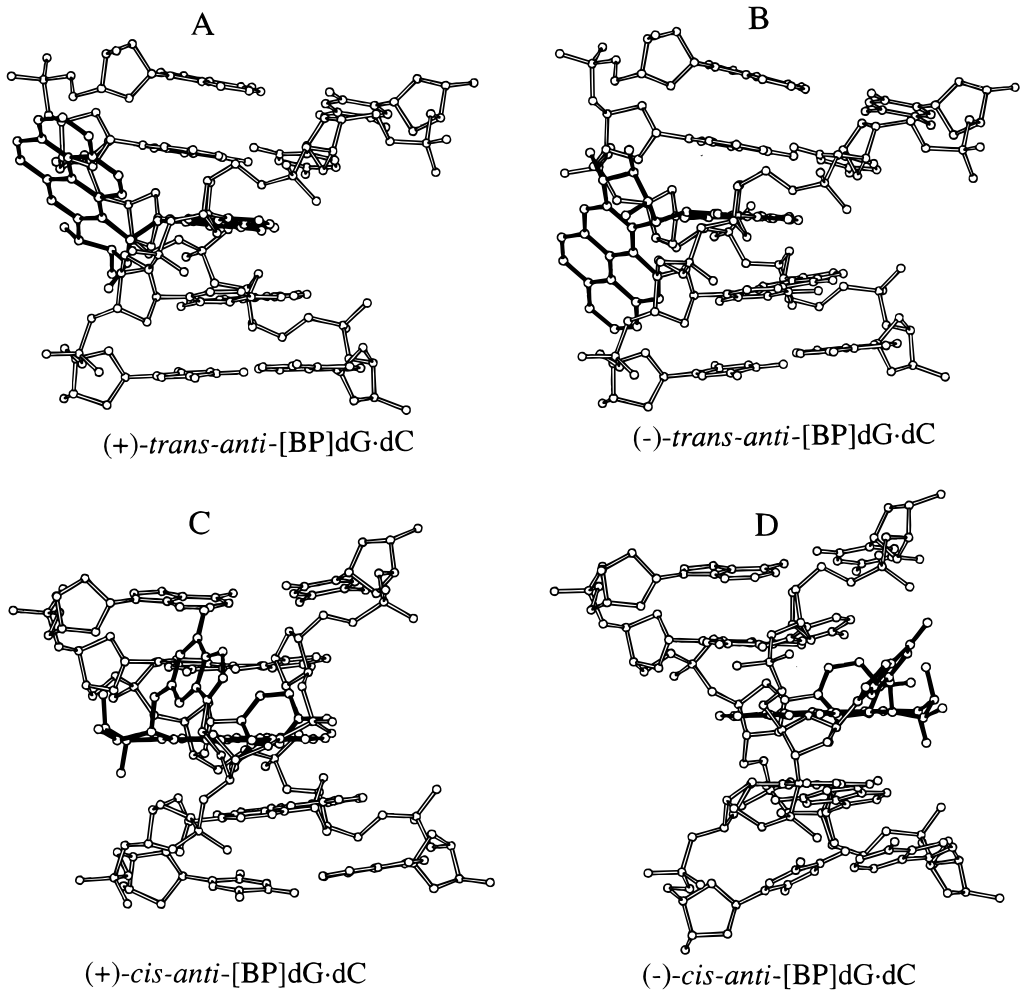

FIGURE 7: Comparative views normal to the helix axis of the d(T4-C5-[BP]G6-C7-T8)·d(A15-G16-C17-G18-A19) segments of the solution structures of the stereomeric (A) (+)-*trans*-*anti*-[BP]dG·dC 11-mer duplex (Cosman et al., 1992), (B) (−)-*trans*-*anti*-[BP]dG·dC 11-mer duplex (de los Santos et al., 1992), (C) (+)-*cis*-*anti*-[BP]dG·dC 11-mer duplex (Cosman et al., 1993), and (D) (−)-*cis*-*anti*-[BP]dG·dC 11-mer duplex (this study). The BP ring system and [BP]dG6 and dC17 bases are shown in darkened bonds. Figures were prepared using Molscript V1.1 (Kraulis, 1991). The stereochemical configuration of the hydroxyl and nitrogen substituents on the BP benzylic ring are shown in Figure 4.

absorbance, linear dichroism, and fluorescence methods, site I was identified as an intercalative conformation with considerable stacking interactions between the pyrenyl residues and DNA bases, while site II was identified as an external adduct conformation (Geacintov et al., 1982). Using site-specific and stereochemically defined *anti*-BPDE-oligodeoxyribonucleotide adducts, it was later demonstrated that *cis*-[BP]dG and *trans*-[BP]dG adducts are associated with site I and site II *anti*-[BP]-DNA adducts, respectively (Geacintov et al., 1991). The structural features of the four stereoisomeric *anti*-[BP]dG·dC 11-mer duplexes described here and based on our NMR studies provide full and detailed descriptions of the conformational features of the site I and site II adducts. The remarkably different base-displaced intercalation (site I) and minor groove (site II) structures are shown to be associated with differences in the absolute steric configurations of substituents about the four chiral 7, 8, 9, and 10 carbon centers. Finally, the *in vivo* less abundant adducts derived from the binding of *anti*-BPDE to the exocyclic amino group of adenine appear to be also intercalative in nature, and thus of the site I-type (Schurter et al., 1995; Yeh et al., 1995); however, these and the structurally related adenine adducts derived from fjord benzo[*c*]phenanthrene diol epoxides with the complementary dT opposite the modified dA bases are intercalative (site I), but without base displacement (Cosman et al., 1993b, 1995b).

The structural differences of the four diastereomeric (+)-*trans*-, (−)-*trans*-, (+)-*cis*-, and (−)-*cis*-*anti*-[BP]dG·dC 11-mer duplexes briefly outlined above should result in differences in how each of these adduct duplexes would interact with repair proteins and other enzymes in the cell. Recent *in vitro* transcription studies (Choi et al., 1994) and *in vitro* polymerase-catalyzed primer extension reaction studies (Hruszkewycz et al., 1992; Shibutani et al., 1993) using template strands containing site-specifically and stereochemically distinct *anti*-[BP]dG adducts showed that all of the stereoisomers strongly block primer extension. Choi et al. (1994) showed that the order of inhibition of elongation by T7 RNA polymerase was (+)-*trans* > (−)-*trans* > (+)-*cis* > (−)-*cis*, when the amount of full length transcript for each is compared to that obtained for an unmodified template. Hruszkewycz et al. (1992) had found that the inhibition of primer extension using either Sequenase DNA polymerase (version 2) or human DNA polymerase a was greater for the (+)-*cis* adduct than for the (+)-*trans* adduct. Shibutani et al. (1993) also showed that primer extension using the Klenow fragment of *Escherichia coli* was strongly blocked by each of the four *anti*-[BP]dG adducts. However, the

primer could be extended past the (−)-*trans-anti*-[BP]dG adduct with small amounts of dAMP incorporated opposite the lesion. Very small amounts of dAMP opposite the (+)-*cis-anti*-[BP]dG adduct were also observed. In comparison, one- and two-base deletions predominated opposite the (−)-*cis-anti*-[BP]dG adduct, and one-base deletions were also observed to a lesser extent opposite the (+)-*trans-anti*-[BP]-dG adduct. It is interesting to note that the adducts that have the same stereochemistry at the BP(C^{10})-[BP]dG6(N^2) linkage site had similar types of point mutations *in vitro*. Thus, a preference for incorporation of dAMP opposite (−)-*trans*- and (+)-*cis-anti*-[BP]dG adducts was observed, while base deletions predominated in the extended primers that were opposite template strands containing (−)-*cis*- and (+)-*trans-anti*-[BP]dG adducts (Shibutani et al., 1993).

Homologous Structures among Benzo[a]pyrenyl Diol Epoxide-DNA Adducts. To date, we can identify several families of DNA adduct structures consisting of members having common conformational features. For example, the (+)-*trans-anti*-[BP]dG (Cosman et al., 1992; Fountain & Krugh, 1995) and (−)-*trans-anti*-[BP]dG (de los Santos et al., 1992) opposite dC adduct duplexes as well as the (−)-*trans-anti*-5-methyl-chrysenyl-N^2-dG opposite dC adduct duplex (Cosman et al., 1995b) belong to the family of structures in which the B-DNA helix is minimally disturbed and the covalently attached ligand resides in the minor groove. A second family of structures includes the (+)- and (−)-*trans-anti*-benzo[*c*]phenanthrenyl-N^6-dA opposite dT (Cosman et al., 1993b, 1995b), the (−)-*trans-anti*-[BP]dA·dG (Schurter et al., 1995a), and the (−)-*trans-syn*-[BP]dA·dT (Schurter et al., 1995b) adduct duplexes, in which the ligand intercalates either to the 5′- or 3′-side of the modified base without disruption of the hydrogen bonding of the modified base pair. A third family of structures, consisting of the (+)-*cis-anti*-[BP]dG adduct opposite dC (Cosman et al., 1993a) or a deletion site (Cosman et al., 1994b) as well as the (+)-*trans-anti*-[BP]dG opposite a deletion site (Cosman et al., 1994a) have structures in which the ligand intercalates into the helix by displacing the modified base into either the minor or major groove. The NMR energy-minimized structure of the (−)-*cis-anti*-[BP]dG·dC 11-mer duplex (present study) belongs to latter structural family in which the covalently attached benzo[*a*]pyrenyl ring intercalates between intact flanking dG·dC base pairs with concurrent displacement of the modified deoxyguanosine into the major groove.

Comparison views looking into the minor groove of the (+)-*trans-anti*-[BP]dG·del and (−)-*cis-anti*-[BP]dG·dC adduct duplexes are shown in Supporting Information Figure S3 and emphasize that the hydrophobic pyrenyl aromatic rings intercalate into the helix. In addition, the orientations of the BP and displaced modified deoxyguanosine base are very similar in the structures of the two benzo[*a*]pyrenyl adduct duplexes, in that the $C^{10}-C^{11}$ bay region containing edge of the BP ring is oriented toward the modified strand and the glycosidic torsion χ angles of the modified dG residues are in the high *anti* domain in both cases.

Conclusions. A striking principal that has emerged from our NMR−molecular mechanics structural studies of stereochemically defined polycyclic aromatic hydrocarbon (PAH)-derived DNA adduct duplexes with their normal complementary strands is the opposite orientations of the covalently attached PAH ligands in pairs of adducts in which the stereochemistry of the substituents at each benzylic ring carbon is inverted. The benzo[*a*]pyrenyl and 5-methylchrysenyl rings in the solution structures of the (+)- and (−)-*trans-anti*-[BP]dG·dC and [MC]dG·dC 11-mer duplexes are located in the minor grooves of minimally perturbed B-DNA duplexes, yet the covalently attached ligands are directed toward either the 5′-end or 3′-end [(+)- and (−)-adducts, respectively] of the modified strand depending on the stereochemistry (Cosman et al., 1992, 1995b; de los Santos et al., 1992). In addition, the benzo[*c*]phenanthrenyl rings which are covalently attached to the N^6 position of deoxyadenosine in the stereomeric (+)- and (−)-*trans-anti*-[BPh]-dA·dT adduct duplexes intercalate either to the 5′ or 3′-side, respectively, without disruption of the hydrogen bonding alignments of the modified [BPh]dA·dT base pair (Cosman et al., 1993b, 1995a). Finally, the benzo[*a*]pyrenyl ring intercalates into the helix by displacing the modified deoxyguanosine and attached benzylic ring either into the minor groove or major groove in the solution structures of the stereomeric (+)- and (−)-*cis-anti*-[BP]dG·dC 11-mer duplexes, respectively.

SUPPORTING INFORMATION AVAILABLE

Five tables listing the complete exchangeable and nonexhangeable proton chemical shifts for the (−)-*cis-anti*-[BP]-dG·dC 11-mer duplex, chemical shift differences between the (−)-*cis-anti*-[BP]dG·dC 11-mer duplex and control 11-mer duplex, and the backbone torsion angles for the central 5-mer segment, and comparison of the magnitude of adjacent residue nucleic acid NOEs in the 5-mer segment with interproton distances observed for the NMR energy-minimized structure, and three figures showing an expanded NOESY contour plot of the adduct duplex in H_2O buffer, plots of the base pair buckle and propeller twist values and the twist angles and rise distances between flanking bases for the entire adduct duplex, and comparison views of the (+)-*trans-anti*-[BP]dG·del and (−)-*cis-anti*-[BP]dG·dC adduct duplexes (10 pages). Ordering information is given on any current masthead page.

REFERENCES

Altona, C., & Sundaralingam, M. (1972) *J. Am. Chem. Soc. 94*, 8205−8212.

Arce, G. T., & Grunberger, D. (1983) *Mutat. Res. 109*, 183−193.

Arce, G. T., Allen, J. W., Doerr, C. L. Elmore, E., Hatch, G. G., Moore, M. M., Sharief, Y., Grunberger, D., & Nesnow, S. (1987) *Cancer Res. 47*, 3388−3395.

Arnott, S., Bond, P. J., Selsing, E., & Smith, P. J. (1976) *Nucleic Acids Res. 2*, 2459−2470.

Ashurst, S. W., Cohen, G. M., Nesnow, S., DiGiovanni, J., & Slaga, T. J. (1983) *Cancer Res. 43*, 1024−1029.

Babcock, M. S., Pednault, E. P. D., & Olson, W. K. (1993) *J. Biomol. Struct. Dyn. 11*, 597−628.

Barton, J. K. (1989) *Pure Appl. Chem. 61*, 563−564.

Berman, H. M., Olson, W. K., Beveridge, D. L., Westbrook, J., Gelbin, A., Demeny, T., Hsieh, S. H., Srinivasan, A. R., & Schneider, B. (1992) *Biophys. J. 63*, 751−759.

Brookes, P., & Osborne, M. R. (1982) *Carcinogenesis 3*, 1223−1226.

Buening, M. K., Wislocki, P. G., Levin, W., Yagi, H., Thakker, D. R., Akagi, H., Koreeda, M., Jerina, D. M., & Conney, A. H. (1978) *Proc. Natl. Acad. Sci. U.S.A. 75*, 5358−5361.

Campbell, D. B., & Wilson, K. (1991) *Biochem. Soc. Trans. 119*, 472−475.

Cheng, S. C., Hilton, B. D., Roman, J. M., & Dipple, A. (1989) *Chem. Res. Toxicol. 2*, 334−340.

Choi, D.-J., Marino-Alessandri, J. F., Geacintov, N. E., & Scicchitano, D. A. (1994) *Biochemistry 33*, 780−787.
Conney, A. H. (1982) *Cancer Res. 42*, 4875−4917.
Cosman, M., Ibanez, V., Geacintov, N. E., & Harvey, R. G. (1990) *Carcinogenesis 11*, 1667−1672.
Cosman, M., de los Santos, C., Fiala, R., Hingerty, B. E., Singh, S., Ibanez, V., Margulis, L., Live, D., Geacintov, N. E., Broyde, S., & Patel, D. J. (1992) *Proc. Natl. Acad. Sci. U.S.A. 89*, 1914−1918.
Cosman, M., de los Santos, C. Fiala, R., Hingerty, B. E., Ibanez, V., Luna, E., Harvey, R., Geacintov, N. E., Broyde, S., & Patel, D. J. (1993a) *Biochemistry 32*, 4146−4155.
Cosman, M., Fiala, R., Hingerty, B. E., Laryea, A., Lee, H., Harvey, R. G., Amin, S., Geacintov, N. E., Broyde, S., & Patel, D. J. (1993b) *Biochemistry 32*, 12488−12497.
Cosman, M., Fiala, R., Hingerty, B. E., Amin, S., Geacintov, N. E., Broyde, S., & Patel, D. J. (1994a) *Biochemistry 33*, 11507−11517.
Cosman, M., Fiala, R., Hingerty, B. E., Amin, S., Geacintov, N. E., Broyde, S., & Patel, D. J. (1994b) *Biochemistry 33*, 11518−11527.
Cosman, M., Laryea, A., Fiala, R., Hingerty, B. E., Amin, S., Geacintov, N. E., Broyde, S., & Patel, D. J. (1995a) *Biochemistry 34*, 1295−1307.
Cosman, M., Xu, R., Hingerty, B. E., Amin, S., Harvey, R. G., Geacintov, N. E., Broyde, S., & Patel, D. J. (1995b) *Biochemistry 34*, 6247−6260.
Cosman, M., Hingerty, B. E., Geacintov, N. E., Broyde, S., & Patel, D. J. (1995c) *Biochemistry 34*, 15334−15350.
de los Santos, C., Cosman, M., Hingerty, B. E., Ibanez, V., Margulis, L., Geacintov, N. E., Broyde, S., & Patel, D. J. (1992) *Biochemistry 31*, 5245−5252.
Fountain, M. A., & Krugh, T. R. (1995) *Biochemistry 34*, 3152−3161.
Geacintov, N. E., Gagliano, A. G., Ibanez, V., & Harvey, R. G. (1982) *Carcinogenesis 3*, 247−253.
Geacintov, N. E., Cosman, M., Mao, B., Alfano, A., Ibanez, V., & Harvey, R. G. (1991) *Carcinogenesis 12*, 2099−2108.
Hare, D. R., Wemmer, D. E., Chou, S. H., Drobny, G., & Reid, B. R. (1983) *J. Mol. Biol. 171*, 319−336.
Harvey, R. G., & Geacintov, N. E. (1988) *Acc. Chem. Res. 21*, 66−73.
Hingerty, B. E., Figueroa, S., Hayden, T., & Broyde, S. (1989) *Biopolymers 28*, 1195−1222.
Hruszkewcz, A. M., Canella, K. A., Peltonen, K., Lotrappa, L., & Dipple, A. (1992) *Carcinogenesis 13*, 2347−2352.
Jeffrey, A. M., Jennette, K. W., Blobstein, S. H., Weinstein, I. B., Beland, F. A., Harvey, R. G., Kasai, H., Miura, I., & Nakanishi, L. (1976) *J. Am. Chem. Soc. 98*, 5714−5715.
Kapitulnik, J., Wislocki, P. G., Levin, W., Yagi, H., Jerina, D. M., & Conney, A. H. (1978) *Cancer Res. 38*, 354−358.
Kraulis, P. J. (1991) *J. Appl. Crystallogr. 24*, 946−950.
Levin, W., Wood, A. W., Yagi, H., Jerina, D. M., & Conney, A. H. (1976) *Proc. Natl. Acad. Sci. U.S.A. 73*, 3867−3871.
Marion, D., Ikura, M., Tschudin, R., & Bax, A. (1989) *J. Magn. Reson. 85*, 393−399.
Meehan, T., & Straub, K. (1979) *Nature 277*, 410−412.
Osborne, M. R., Jacobs, S., Harvey, R. G., & Brooks, P. (1976) *Int. J. Cancer 1*, 362−368.
Patel, D. J., Kozlowski, S. A., Nordheim, A., & Rich, A. (1982) *Proc. Natl. Acad. Sci. U.S.A. 79*, 1413−1417.
Patel, D. J., Shapiro, L., & Hare, D. (1987) *Annu. Rev. Biophys. Biophys. Chem. 16*, 423−454.
Phillips, D. H. (1983) *Nature 303*, 468−472.
Quigley, G. J., Wang, A. H.-J., Ughetto, G., van der Marel, G., van Boom, J. H., & Rich, A. (1980) *Proc. Natl. Acad. Sci. U.S.A. 77*, 7204−7208.
Saenger, W. (1980) *Principles of Nucleic Acid Structure*, pp 360−361, Springer-Verlag, New York.
Schurter, E. J., Yeh, H. J. C., Sayer, J. M., Lakshman M. K., Yagi, H., Jerina, D. M., & Gorenstein, D. G. (1995a) *Biochemistry 34*, 1364−1375.
Schurter, E. J., Sayer, J. M., Oh-Hara, T., Yeh, H. J. C., Yagi, H., Luxon, B. A., Jerina, D. M., & Gorenstein, D. G. (1995b) *Biochemistry 34*, 9009−9020.
Seiler, J. P. (1990) *Mutat. Res. 245*, 165−169.
Shapiro, R., Hingerty, B. E., & Broyde, S. (1989) *J. Biomol. Struct. Dyn. 7*, 493−513.
Shibutani, S., Margulis, L. A., Geacintov, N. E., & Grollman, A. P. (1993) *Biochemistry 32*, 7531−7541.
Sims, P., Grover, P. L., Swaisland, A., Pal, K., & Hewer, A. (1974) *Nature 252*, 326−328.
Singer, B., & Grunberger, D. (1983) *Molecular Biology of Mutagens and Carcinogens*, Plenum Press, New York.
Singh, S. B., Hingerty, B. E., Singh, U. C., Greenberg, J. P., Geacintov, N. E., & Broyde, S. (1991) *Cancer Res. 51*, 3482−3492.
Slaga, T. J., Bracken, W. J., Gleason, G., Levin, W., Yagi, H., Jerina, D. M., & Conney, A. H. (1979) *Cancer Res. 39*, 67−71.
Stevens, C. W., Bouck, N., Burgess, J. A., & Fahl, W. E. (1985) *Mutat. Res. 152*, 5−14.
Stinson, S. C. (1995) *Chem. Eng. News 73*, 44−74.
Taylor, E. R., & Olson, W. K. (1983) *Biopolymers 22*, 2667−2702.
Testa, B. (1989) *Chirality 1*, 7−9.
van der Ven, F. J., & Hilbers, C. W. (1988) *Eur. J. Biochem. 178*, 1−38.
Wood, A. W., Chang, L. R., Levin, W., Yagi, H., Thakker, D. R., Jerina, D., & Conney, A. H. (1977) *Biochem. Biophys. Res. Commun. 77*, 1389−1396.
Ya, N. Q., Smirnov, S., Cosman, M., Bhanot, S., Ibanez, V., & Geacintov, N. E. (1994) *Structural Biology: The State of the Art* (Sarma, R. H., & Sarma, M., Eds.) Adenine Press, Schenectady, NY.
Yeh, H. J., Sayer, J. M., Liu, X., Altieri, A. S., Byrd, R. A., Lakshman, M. K., Yagi, H., Schurter, E. J., Gorenstein, D. G., & Jerina, D. M. (1995) *Biochemistry 34*, 13570−13581.

BI9605346